

# Parallel Multi-Coordinate Descent Methods for Full Configuration Interaction

Yuejia Zhang,<sup>†</sup> Weiguo Gao,<sup>\*,†,‡,¶</sup> and Yingzhou Li<sup>\*,†</sup>

<sup>†</sup>*School of Mathematical Sciences, Fudan University, Shanghai, China*

<sup>‡</sup>*School of Data Science, Fudan University, Shanghai, China*

<sup>¶</sup>*Shanghai Artificial Intelligence Laboratory, Shanghai, China*

E-mail: wggao@fudan.edu.cn; yingzhouli@fudan.edu.cn

## Abstract

We develop a multi-threaded parallel coordinate descent full configuration interaction algorithm (mCDFCI), for the electronic structure ground-state calculation in the configuration interaction framework. The FCI problem is reformulated as an unconstrained minimization problem, and tackled by a modified block coordinate descent method with a deterministic compression strategy. mCDFCI is designed to prioritize determinants based on their importance, with block updates enabling efficient parallelization on shared-memory, multi-core computing infrastructure. We demonstrate the efficiency of the algorithm by computing an accurate benchmark energy for the chromium dimer in the Ahlrichs SV basis (48e, 42o), which explicitly includes  $2.07 \times 10^9$  variational determinants. We also provide the binding curve of the nitrogen dimer under the cc-pVQZ basis set (14e, 110o). Benchmarks show up to 79.3% parallel efficiency on 128 cores.

## 1 Introduction

Understanding the chemical properties of molecules relies on solving the many-body time-independent electronic Schrödinger equation. However, traditional methods, such as density functional theory (DFT) or coupled-cluster with single, double, and perturbative triple excitations (CCSD(T)), often struggle

to accurately describe the electronic structure of strongly correlated systems. This limitation is particularly evident in molecules with transition metals or those in non-equilibrium geometries.

Full configuration interaction (FCI) provides a numerically exact solution under a predefined basis set by describing the wavefunction as a superposition of all possible Slater determinants. However, FCI methods scale exponentially with the number of orbitals and electrons, leading to the curse of dimensionality. To leverage this challenge and apply FCI methods to large systems, it becomes necessary to compress the wavefunction. This can be achieved by employing different wavefunction ansätze, such as the matrix product state (MPS) in the density matrix renormalization group (DMRG) method,<sup>1-5</sup> or by representing the wavefunction as a population of random particles, as in the full configuration interaction quantum Monte Carlo (FCIQMC) method.<sup>6-10</sup> Another approach involves selecting important Slater determinants, guided by the extensive sparsity of the FCI wavefunction.<sup>11</sup> The method we describe in this paper falls into this category, which is known as selected CI method.

A variety of selected CI methods have been developed, starting from the earliest work in 1973 known as Configuration Interaction using a Perturbative Selection done Iteratively (CIPSI),<sup>12</sup> to recent advancements including Adaptive Sampling CI (ASCI),<sup>13</sup> Heat-

bath CI (HCI),<sup>14</sup> Semistochastic Heat-bath CI (SHCI),<sup>15,16</sup> Coordinate Descent FCI (CD-FCI),<sup>17</sup> Fast Randomized Iteration method for FCI (FCI-FRI),<sup>18</sup> Reinforcement Learning CI (RLCI),<sup>19</sup> and others. These methods share the common iterative approach of expanding a primary configuration space, filtering determinants based on some importance estimate, and computing the leading eigenpair to obtain an enhanced approximation of the wavefunction until convergence is achieved. Typically, Epstein–Nesbet second-order perturbation theory is further employed in the secondary space to account for the remaining correlation that is not captured by the variational SCI treatment. Selected CI variants significantly reduce the computational cost of FCI by diminishing the dimension of the primary SCI space compared to the  $N$ -electron Hilbert space, while they differ by having distinct selection principles and implementations.

This paper extends the coordinate descent FCI (CDFCI)<sup>17</sup> method previously proposed by one of our authors and his collaborators, which provides selection rules from an optimization perspective. Initially, it transforms the FCI eigenvalue problem into an unconstrained minimization problem, with local minima corresponding to the ground state of the system. Next, it employs the coordinate descent method for the following advantages: (i) The gradient of the objective function provides a natural determinant selection rule, adding important determinants into the variational space until it reaches the memory limit; (ii) The special structure of the problem allows us to perform an exact line search, accelerating the energy convergence; (iii) In each iteration, updating only one coordinate of the optimization vector involves only one column of the Hamiltonian matrix, avoiding operations with the entire Hamiltonian matrix, thus reducing the computation cost associated with unappreciative determinants. The CDFCI method obtains the ground-state energy and wavefunction without explicitly extracting the Hamiltonian submatrix for direct diagonalization. This makes immense room for the storage of the wavefunction, making it possible for larger systems and more

accurate approximations. The effective determinant selection rule and the low storage cost are the main reasons why CDFCI becomes a competitive FCI solver.

Although CDFCI demonstrates accelerated performance in experiments, its parallelization capability is restricted by the inherent sequential nature of the method. In this paper, we present a novel algorithm to address the minimization problem, which extends update of one coordinate to multiple coordinates per iteration. To achieve this, the algorithm introduces an additional search dimension to enable the exact line search. This extension not only accelerates convergence but also opens up new possibilities for parallelization. Benefiting from fully parallelizable coordinate updates, our new algorithm achieves an accuracy of  $10^{-5}$  Ha for  $C_2$  and  $N_2$  using the cc-pVDZ basis in 10 and 30 minutes respectively, nearly twenty times faster than the single-threaded version reported in the original CDFCI work. When compared to the multi-threaded version of the original CDFCI that supports parallel hashtable updates, our algorithm delivers a  $3.0\times$  speedup. Additionally, it computes the ground state of all-electron  $Cr_2$  with Ahlrichs SV basis in 5.8 days, matching the accuracy of the original CDFCI, which previously required one month for the same task.

In the rest of this paper, we present the algorithm in section 2 and discuss the implementation details in section 3. In section 4, we demonstrate the accuracy and the parallel efficiency of our method by applying it to various molecules including  $C_2$ ,  $N_2$  and  $Cr_2$ . The binding curve of  $N_2$  under cc-pVQZ basis is also characterized. Finally, we conclude and look ahead to future work in section 5.

## 2 Methodology and Approach

In this section, we begin by reviewing the reformulation of the FCI eigenvalue problem as a nonconvex optimization problem.<sup>17,20</sup> Following this, we describe in detail the multi-coordinate descent methods to address the FCI problem.

## 2.1 Problem Formulation

With a complete set of one-electron spin-orbitals  $\{\chi_p\}$ , the many-body Hamiltonian operator can be expressed using second quantization as follows:

$$\hat{H} = \sum_{p,q} t_{pq} \hat{a}_p^\dagger \hat{a}_q + \frac{1}{2} \sum_{p,q,r,s} v_{pqrs} \hat{a}_p^\dagger \hat{a}_q^\dagger \hat{a}_s \hat{a}_r, \quad (1)$$

where  $\hat{a}_p^\dagger$  and  $\hat{a}_p$  represent the creation and annihilation operators, respectively, for spin-orbital  $p$ . The coefficients  $t_{pq}$  and  $v_{pqrs}$  correspond to one- and two-electron integrals. The ground-state energy of  $\hat{H}$  is determined by solving the time-independent Schrödinger equation:

$$\hat{H} |\Phi_0\rangle = E_0 |\Phi_0\rangle, \quad (2)$$

where  $E_0$  represents the ground-state energy, i.e., the lowest eigenvalue of  $\hat{H}$ , and  $|\Phi_0\rangle$  is the associated ground-state wavefunction. We assume, without loss of generality, that  $E_0$  is negative and non-degenerate, meaning the eigenvalues of  $\hat{H}$  are ordered as  $E_0 < E_1 \leq E_2 \leq \dots$ .

The full configuration interaction (FCI) method starts from a truncated finite spin-orbital subset  $\{\chi_p\}_{p=1}^{n_{\text{orb}}}$ , where  $n_{\text{orb}}$  denotes the number of orbitals, and this subset is usually obtained from a Hartree–Fock procedure. The wavefunction is approximated as a linear combination of Slater determinants,

$$|\Phi_0\rangle = \sum_{i=1}^{N_{\text{FCI}}} c_i |D_i\rangle = \sum_{i=1}^{N_{\text{FCI}}} c_i |\chi_{i_1} \chi_{i_2} \cdots \chi_{i_n}\rangle, \quad (3)$$

with  $1 \leq i_1 < i_2 < \dots < i_n \leq n_{\text{orb}}$ . Here,  $n = n_{\text{elec}}$  denotes the number of electrons in the system, and  $N_{\text{FCI}}$  is the dimension of FCI variational space, which represents the total number of configurations, and is of order  $\mathcal{O}\left(\binom{n_{\text{orb}}}{n_{\text{elec}}}\right)$ .

Following this, the Schrödinger equation (2) is discretized into a matrix eigenvalue problem

$$H\mathbf{c} = E_0\mathbf{c}, \quad (4)$$

where  $H$  is a real symmetric  $N_{\text{FCI}} \times N_{\text{FCI}}$  matrix, with entry  $H_{i,j} = \langle D_i | \hat{H} | D_j \rangle$ , and  $\mathbf{c}$  is a vector of dimension  $N_{\text{FCI}}$ , with entry  $c_i$ . The problem (4) is known as the FCI eigenvalue prob-

lem.

The second-quantized Hamiltonian operator defined in (1) signifies that  $H_{i,j}$  is zero if transforming  $|D_i\rangle$  into  $|D_j\rangle$  involves altering more than two occupied spin-orbitals. Consequently,  $H$  has  $\mathcal{O}(n_{\text{elec}}^2 n_{\text{orb}}^2)$  non-zero entries per row, which is much smaller than  $N_{\text{FCI}}$  in terms of order, thus leading to an extreme sparsity structure in the matrix  $H$ .

Selected CI methods<sup>12–15</sup> target a submatrix of  $H$  and use its lowest eigenpair as an estimate to the FCI eigenvalue problem. Now, instead of doing direct diagonalization to the submatrix of  $H$ , we consider the following optimization problem

$$\min_{\mathbf{c} \in \mathbb{R}^{N_{\text{FCI}}}} f(\mathbf{c}) = \min_{\mathbf{c}} \|H + \mathbf{c}\mathbf{c}^\top\|_{\text{F}}^2 \quad (5)$$

with the same Hamiltonian matrix  $H$  as defined above. The gradient of the objective function is

$$\nabla f(\mathbf{c}) = 4H\mathbf{c} + 4(\mathbf{c}^\top \mathbf{c})\mathbf{c}. \quad (6)$$

It is shown that<sup>20</sup>  $\pm\sqrt{-E_0}\mathbf{v}_0$  are the only two local minimizers, where  $\mathbf{v}_0$  is the normalized eigenvector corresponding to the smallest eigenvalue  $E_0 < 0$ . Suppose we have an estimate  $\hat{\mathbf{c}}$  to the solution  $\mathbf{c}^*$  of problem (5), by simply normalizing  $\hat{\mathbf{c}}$ , we can obtain an approximate solution of the FCI eigenvalue problem.

In this work, we follow the idea of coordinate descent, extend one coordinate update per iteration to multiple coordinates, and add an additional scaling factor to enable exact line search, which is undoubtedly more beneficial to convergence. We also follow the compression strategy in CDFCI, which improves the efficiency of the algorithm and controls the memory footprint so that CDFCI can converge in a subspace. Below we describe our algorithm in detail.

## 2.2 Algorithm

The multi-coordinate descent method is an iterative optimization technique similar to the original coordinate descent method. However, instead of modifying a single coordinate of the optimization variable  $\mathbf{c}$  in each iteration, we update  $k$  coordinates simultaneously and intro-

duce a scaling factor  $\gamma$ .

Let us denote  $\mathbf{c}^{(\ell)}$  as the vector  $\mathbf{c}$  at the current iteration  $\ell$ . We also define  $\mathcal{I}^{(\ell)} = \{i_1^{(\ell)}, \dots, i_k^{(\ell)}\} \subset \{1, \dots, N_{\text{FCI}}\}$  as the set of  $k$  distinct coordinates chosen for the update in this iteration.

The update rule for each component of  $\mathbf{c}$  is given by:

$$c_i^{(\ell+1)} \leftarrow \begin{cases} \gamma^{(\ell)} c_i^{(\ell)} + a_i^{(\ell)}, & \text{if } i \in \mathcal{I}^{(\ell)}, \\ \gamma^{(\ell)} c_i^{(\ell)}, & \text{otherwise.} \end{cases} \quad (7)$$

where  $\gamma^{(\ell)}$  is a scaling factor, and  $a_i^{(\ell)}$  is the corresponding step size. Each entry  $c_i^{(\ell)}$  is initially scaled by  $\gamma^{(\ell)}$ . For the specific coordinates  $i$  included in the set  $\mathcal{I}^{(\ell)}$ ,  $c_i^{(\ell)}$  is then further updated by adding a step size to the current value.

In matrix form, the update rule can be expressed as:

$$\mathbf{c}^{(\ell+1)} \leftarrow \gamma^{(\ell)} \mathbf{c}^{(\ell)} + \mathcal{E}_{\mathcal{I}^{(\ell)}} \mathbf{a}^{(\ell)}, \quad (8)$$

where  $\mathcal{E}_{\mathcal{I}} \in \mathbb{R}^{N_{\text{FCI}} \times k}$  is defined as  $\mathcal{E}_{\mathcal{I}} = [e_{i_1}, \dots, e_{i_k}]$ , with  $\mathcal{I} = \{i_1, \dots, i_k\}$  and  $1 \leq i_j \leq N_{\text{FCI}}$ . In other words,  $\mathcal{E}_{\mathcal{I}}$  consists of columns from the identity matrix corresponding to the selected coordinates. Essentially, it projects the elements of  $\mathbf{a}^{(\ell)} \in \mathbb{R}^k$  into the higher-dimensional space of  $\mathbf{c}^{(\ell)} \in \mathbb{R}^{N_{\text{FCI}}}$ , inserting zeros for the coordinates not included in  $\mathcal{I}^{(\ell)}$ .

In section 2.2.1, we discuss how we select the  $k$  coordinates in each iteration. Next, in section 2.2.2, we explain how we choose the scaling scalar  $\gamma^{(\ell)}$  and the stepsize vector  $\mathbf{a}^{(\ell)}$ , so that they give the best descent value in the objective function. Each local update actually provides an energy estimate for the global problem.

Following the algorithmic design in CDFCI,<sup>20</sup> we store an additional vector  $\mathbf{b}$  in memory, which approximates  $H\mathbf{c}$  with differences only in the coordinates that are compressed. This will facilitate both picking coordinates and choosing the stepsize. In section 2.2.3, we show how we update  $\mathbf{b}$  and  $\mathbf{c}$  as well as other quantities after each iteration, where we insert a compression strategy that keeps the memory footprint affordable. Finally, in section 2.2.4, we provide the complete pseudocode, along with a dis-

ussion of possible choices for initialization and stopping criteria.

## 2.2.1 Coordinate Selection

The selection rule of coordinates follows the largest gradients rule: the  $k$  coordinates with largest absolute value of (6) are considered. In other words, choose  $k$  coordinates, in which

$$i_j = \arg \max_{i \neq i_1, \dots, i_{j-1}} |[\nabla f(\mathbf{c})]_i|, \quad j = 1, \dots, k, \quad (9)$$

where  $[\nabla f(\mathbf{c})]_i$  denotes the  $i$ -th coordinate of  $\nabla f(\mathbf{c}) = 4H\mathbf{c} + 4(\mathbf{c}^T \mathbf{c})\mathbf{c}$ .

Since in the algorithm design, the vector  $\mathbf{b}$  is stored as a compressed representation of  $H\mathbf{c}$ , at iteration  $\ell$ , the approximated gradient of the objective function can be easily obtained by a linear combination of  $\mathbf{b}^{(\ell)}$  and  $\mathbf{c}^{(\ell)}$ . In addition, we consider only the determinant set  $\mathcal{I}_H(\mathcal{I}^{(\ell)})$  which is defined as:

$$\mathcal{I}_H(\mathcal{I}^{(\ell)}) := \{1 \leq i \leq N_{\text{FCI}} : \exists j \in \mathcal{I}^{(\ell)} \text{ such that } H_{i,j} \neq 0\},$$

where  $\mathcal{I}^{(\ell)}$  denotes the set of coordinates selected during the  $\ell$ -th iteration.

Therefore, the actual coordinate selection rule at iteration  $\ell$  is

$$i_j^{(\ell)} = \arg \max_{\substack{i \in \mathcal{I}_H(\mathcal{I}^{(\ell-1)}) \\ i \neq i_1^{(\ell)}, \dots, i_{j-1}^{(\ell)}}} \left| 4b_i^{(\ell)} + 4((\mathbf{c}^{(\ell)})^T \mathbf{c}^{(\ell)}) c_i^{(\ell)} \right|, \quad j = 1, \dots, k. \quad (10)$$

Our coordinate selection method is built on the concept of an active space, which is a carefully chosen subset of the full configuration space. This active space includes only the most important determinants, that are expected to contribute the most to the solution. To construct this space efficiently, we limit our consideration to determinants that are connected to the current iterate by the creation or annihilation of up to two electrons. This restriction helps to avoid including determinants that are far removed in configuration space, which would contribute minimally to the final solution. This approach enhances computational efficiency by

focusing resources on the most relevant determinants, ensuring that the optimization process is both effective and efficient.

### 2.2.2 Optimal Scaling and Stepsize Selection

Once we have selected  $\mathcal{I}^{(\ell)}$ , the  $k$  coordinates to update, we minimize the objective function with respect to the scaling scalar  $\gamma^{(\ell)}$  and the stepsize vector  $\mathbf{a}^{(\ell)}$ :

$$f(\mathbf{c}^{(\ell+1)}) = \left\| H + \mathbf{c}^{(\ell+1)}(\mathbf{c}^{(\ell+1)})^T \right\|_{\text{F}}^2, \quad (11)$$

where  $\mathbf{c}^{(\ell+1)} = \gamma^{(\ell)}\mathbf{c}^{(\ell)} + \mathcal{E}_{\mathcal{I}^{(\ell)}}\mathbf{a}^{(\ell)}$ . In the following, we describe how we perform an exact line search in a  $(k+1)$ -dimensional subspace so that  $\gamma^{(\ell)}$  and  $\mathbf{a}^{(\ell)}$  are both globally optimal.

Let  $\mathbf{y}^{(\ell)} = \mathbf{c}^{(\ell)} - \mathcal{E}_{\mathcal{I}^{(\ell)}}(\mathcal{E}_{\mathcal{I}^{(\ell)}})^T\mathbf{c}^{(\ell)}$ , which sets the entries in coordinate set  $\mathcal{I}^{(\ell)}$  to zeros. Define

$$\tilde{\mathbf{y}}^{(\ell)} = \begin{cases} \mathbf{y}^{(\ell)} / \|\mathbf{y}^{(\ell)}\|, & \text{if } \|\mathbf{y}^{(\ell)}\| \neq 0, \\ 0, & \text{otherwise,} \end{cases}$$

so that we always have  $\mathbf{y}^{(\ell)} = \tilde{\mathbf{y}}^{(\ell)}\|\mathbf{y}^{(\ell)}\|$  regardless of whether  $\|\mathbf{y}^{(\ell)}\| = 0$ .

The update of  $\mathbf{c}$  given in (8) can be rewritten as

$$\begin{aligned} \mathbf{c}^{(\ell+1)} &= \gamma^{(\ell)}\mathbf{c}^{(\ell)} + \mathcal{E}_{\mathcal{I}^{(\ell)}}\mathbf{a}^{(\ell)} \\ &= Q^{(\ell)}\mathbf{z}^{(\ell)}, \end{aligned} \quad (12)$$

with  $Q^{(\ell)}$  and  $\mathbf{z}^{(\ell)}$  defined as follows:

$$Q^{(\ell)} := [\tilde{\mathbf{y}}^{(\ell)} \quad \mathcal{E}_{\mathcal{I}^{(\ell)}}] \in \mathbb{R}^{N_{\text{FCI}} \times (k+1)}, \quad (13)$$

$$\mathbf{z}^{(\ell)} := \begin{bmatrix} \gamma^{(\ell)}\|\mathbf{y}^{(\ell)}\| \\ \gamma^{(\ell)}(\mathcal{E}_{\mathcal{I}^{(\ell)}})^T\mathbf{c}^{(\ell)} + \mathbf{a}^{(\ell)} \end{bmatrix}. \quad (14)$$

Figure 1 demonstrates how the vector  $\mathbf{c}$  is updated in each iteration.

If  $\|\mathbf{y}^{(\ell)}\| \neq 0$ ,  $Q^{(\ell)}$  is an orthogonal matrix and an orthogonal basis for the  $(k+1)$ -dimensional search space. If  $\|\mathbf{y}^{(\ell)}\| = 0$ ,  $(Q^{(\ell)})^T Q^{(\ell)} = \begin{bmatrix} 0 & \\ & I_k \end{bmatrix}$ , which means the last  $k$  columns of  $Q^{(\ell)}$  form an orthogonal basis for the  $k$ -dimensional search space.

Now consider split the optimization prob-

lem (11) into two parts as follows:

$$\begin{aligned} f(\mathbf{c}^{(\ell+1)}) &= \left\| H + \mathbf{c}^{(\ell+1)}(\mathbf{c}^{(\ell+1)})^T \right\|_{\text{F}}^2 \\ &= \left\| (Q^{(\ell)}(Q^{(\ell)})^T) \left( H + \mathbf{c}^{(\ell+1)}(\mathbf{c}^{(\ell+1)})^T \right) \right\|_{\text{F}}^2 \\ &\quad + \left\| (I - Q^{(\ell)}(Q^{(\ell)})^T) \left( H + \mathbf{c}^{(\ell+1)}(\mathbf{c}^{(\ell+1)})^T \right) \right\|_{\text{F}}^2 \\ &= \left\| (Q^{(\ell)})^T \left( H + \mathbf{c}^{(\ell+1)}(\mathbf{c}^{(\ell+1)})^T \right) Q^{(\ell)} \right\|_{\text{F}}^2 \\ &\quad + \left\| (I - Q^{(\ell)}(Q^{(\ell)})^T) H \right\|_{\text{F}}^2 \\ &= \left\| (Q^{(\ell)})^T H Q^{(\ell)} + \mathbf{z}^{(\ell)}(\mathbf{z}^{(\ell)})^T \right\|_{\text{F}}^2 + \text{constant}. \end{aligned} \quad (15)$$

The third equality follows from the fact that  $(I - Q^{(\ell)}(Q^{(\ell)})^T)\mathbf{c}^{(\ell+1)} = 0$ , and the last equality is derived from equation (12). In addition, the term  $\left\| (I - Q^{(\ell)}(Q^{(\ell)})^T) H \right\|_{\text{F}}^2$  is considered as a constant because it does not depend on  $\mathbf{z}^{(\ell)}$ , and therefore neither on  $\gamma^{(\ell)}$  nor  $\mathbf{a}^{(\ell)}$ .

We choose  $\mathbf{z}^{(\ell)}$  to be the optimal solution to the local minimization problem

$$\begin{aligned} \mathbf{z}^{(\ell)} &= \arg \min_{\mathbf{z} \in \mathbb{R}^{k+1}} f(\mathbf{z}) \\ &= \arg \min_{\mathbf{z} \in \mathbb{R}^{k+1}} \left\| (Q^{(\ell)})^T H Q^{(\ell)} + \mathbf{z}\mathbf{z}^T \right\|_{\text{F}}^2. \end{aligned} \quad (16)$$

The minimum is attained when<sup>20</sup>

$$\mathbf{z}^{(\ell)} = \pm \sqrt{-\lambda^{(\ell)}} \mathbf{v}_{\lambda^{(\ell)}}, \quad (17)$$

where  $\lambda^{(\ell)} := \lambda_{\min}((Q^{(\ell)})^T H Q^{(\ell)})$  is the minimal eigenvalue of matrix  $(Q^{(\ell)})^T H Q^{(\ell)}$  and  $\mathbf{v}_{\lambda^{(\ell)}}$  is the corresponding eigenvector. The eigenvalue  $\lambda^{(\ell)}$  is guaranteed to be negative as long as  $(\mathbf{c}^{(1)})^T H \mathbf{c}^{(1)} < 0$  (see Appendix A for proof and section 2.2.4 for the discussion of initialization).

The problem (16) consists of two parts: assembling the  $(Q^{(\ell)})^T H Q^{(\ell)}$  matrix and calculating its leading eigenpair. To start, we see that,

$$\begin{aligned} &(Q^{(\ell)})^T H Q^{(\ell)} \\ &= \begin{bmatrix} (\tilde{\mathbf{y}}^{(\ell)})^T \\ \mathcal{E}_{\mathcal{I}^{(\ell)}}^T \end{bmatrix} H [\tilde{\mathbf{y}}^{(\ell)} \quad \mathcal{E}_{\mathcal{I}^{(\ell)}}] \\ &= \begin{bmatrix} (\tilde{\mathbf{y}}^{(\ell)})^T H \tilde{\mathbf{y}}^{(\ell)} & (\tilde{\mathbf{y}}^{(\ell)})^T H \mathcal{E}_{\mathcal{I}^{(\ell)}} \\ \mathcal{E}_{\mathcal{I}^{(\ell)}}^T H \tilde{\mathbf{y}}^{(\ell)} & \mathcal{E}_{\mathcal{I}^{(\ell)}}^T H \mathcal{E}_{\mathcal{I}^{(\ell)}} \end{bmatrix}. \end{aligned} \quad (18)$$

If  $\|\mathbf{y}^{(\ell)}\| \neq 0$ , each block is computed as de-

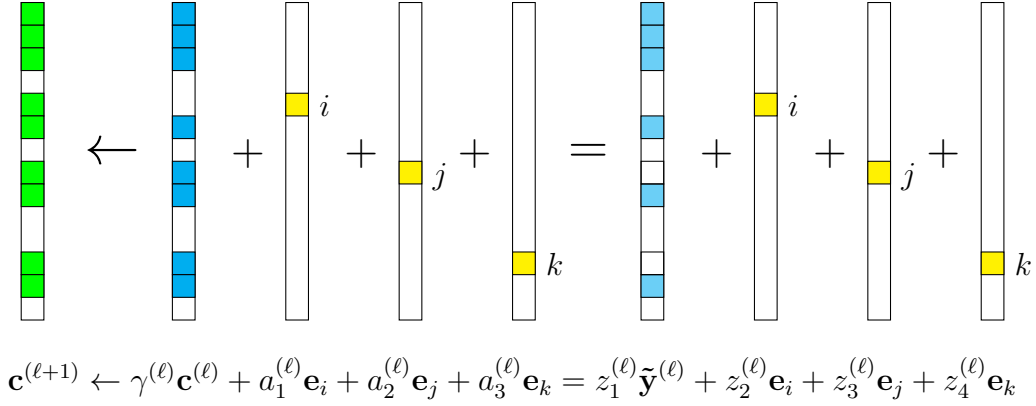


Figure 1: The update of vector  $\mathbf{c}$  when  $k = 3$ . After three coordinates  $i, j, k$  are picked (in yellow), these coordinates of  $\mathbf{c}^{(\ell)}$  are zeroed out and the resulting  $\mathbf{y}^{(\ell)}$  is normalized to  $\tilde{\mathbf{y}}^{(\ell)}$  (in light blue). The coefficients  $a_i^{(\ell)}$  and  $z_i^{(\ell)}$  represent the  $i$ -th element of vectors  $\mathbf{a}^{(\ell)}$  and  $\mathbf{z}^{(\ell)}$  respectively.

scribed below.

1.  $(\tilde{\mathbf{y}}^{(\ell)})^T H \tilde{\mathbf{y}}^{(\ell)} \in \mathbb{R}$ : it is evaluated by  $\frac{1}{\|\mathbf{y}^{(\ell)}\|^2} \left( (\mathbf{c}^{(\ell)})^T \mathbf{b}^{(\ell)} - 2 \sum_{i \in \mathcal{I}^{(\ell)}} c_i^{(\ell)} b_i^{(\ell)} + \sum_{i,j \in \mathcal{I}^{(\ell)}} c_i^{(\ell)} H_{i,j} c_j^{(\ell)} \right)$ .
2.  $((\tilde{\mathbf{y}}^{(\ell)})^T H \mathcal{E}_{\mathcal{I}^{(\ell)}})^T = \mathcal{E}_{\mathcal{I}^{(\ell)}}^T H \tilde{\mathbf{y}}^{(\ell)} \in \mathbb{R}^k$ : its  $i$ -th entry is evaluated by  $\frac{1}{\|\mathbf{y}^{(\ell)}\|} \left( b_i^{(\ell)} - \sum_{j \in \mathcal{I}^{(\ell)}} H_{i,j} c_j^{(\ell)} \right)$ .
3.  $\mathcal{E}_{\mathcal{I}^{(\ell)}}^T H \mathcal{E}_{\mathcal{I}^{(\ell)}} \in \mathbb{R}^{k \times k}$ : It is the submatrix of  $H$  with index set  $\mathcal{I}^{(\ell)}$ . For  $i, j \in \mathcal{I}^{(\ell)}$ , the entry  $H_{i,j}$  is evaluated on the fly by  $H_{i,j} = \langle D_i | \hat{H} | D_j \rangle$ .

In the other case when  $\|\mathbf{y}^{(\ell)}\| = 0$ , only the matrix block  $\mathcal{E}_{\mathcal{I}^{(\ell)}}^T H \mathcal{E}_{\mathcal{I}^{(\ell)}}$  is non-zero.

When  $k$  is not too large, the smallest eigenpair of  $(Q^{(\ell)})^T H Q^{(\ell)}$  can be easily retrieved by default LAPACK eigensolvers<sup>21</sup> for selected eigenvalues. Once this is complete,  $\mathbf{z}^{(\ell)}$  is computed according to equation (17). By equation (14), we have

$$\gamma^{(\ell)} = \begin{cases} \frac{z_1^{(\ell)}}{\|\mathbf{y}^{(\ell)}\|}, & \text{if } \|\mathbf{y}^{(\ell)}\| \neq 0, \\ 1, & \text{otherwise,} \end{cases} \quad (19)$$

and

$$\mathbf{a}^{(\ell)} = \mathbf{z}_2^{(\ell)} - \gamma^{(\ell)} (\mathcal{E}_{\mathcal{I}^{(\ell)}})^T \mathbf{c}^{(\ell)}, \quad (20)$$

where  $z_1^{(\ell)}$  denotes the first entry of  $\mathbf{z}$ , and  $\mathbf{z}_2^{(\ell)} \in \mathbb{R}^k$  the rest of the vector. Note that for the case of  $\|\mathbf{y}^{(\ell)}\| = 0$ ,  $z_1^{(\ell)}$  would always be

zero, and  $\gamma^{(\ell)}$  can be any value. For simplicity, we just set  $\gamma^{(\ell)} = 1$ .

### 2.2.3 Variable Update and Coefficient Compression

After obtaining the scaling factor  $\gamma^{(\ell)}$  and the stepsize  $\mathbf{a}^{(\ell)}$  from the procedure described in section 2.2.2, vectors  $\mathbf{c}$  and  $\mathbf{b}$  are updated by

$$\mathbf{c}^{(\ell+1)} \leftarrow \gamma^{(\ell)} \mathbf{c}^{(\ell)} + \mathcal{E}_{\mathcal{I}^{(\ell)}} \mathbf{a}^{(\ell)}, \quad (21)$$

and

$$\mathbf{b}^{(\ell+1)} \leftarrow \gamma^{(\ell)} \mathbf{b}^{(\ell)} + H \mathcal{E}_{\mathcal{I}^{(\ell)}} \mathbf{a}^{(\ell)}. \quad (22)$$

It should be noted that in the actual implementation,  $\mathbf{c}^{(\ell+1)}$  is not updated exactly as shown above. Instead, we store the scaling factor  $\gamma$  and modify only the relevant entries of  $\mathbf{c}^{(\ell)}$ , while most entries remain unchanged. For a detailed description of the implementation, please refer to section 3.

Through the above update rules (21) and (22), the number of non-zero elements in  $\mathbf{c}$  and  $\mathbf{b}$  will continue to grow. Specifically, the growth rate for  $\mathbf{b}$  is much faster than  $\mathbf{c}$  in the beginning, because the number of entries involved in updating  $\mathbf{b}$  in (22) is much greater than updating  $\mathbf{c}$  in (21). This process can be seen as continuously adding determinants to the variational space, the selected subspace of the full CI space where we approximate the ground state. If we continue to iterate without compression, the variational space will even-

tually expand to the full CI space, which is obviously not feasible for large systems. To this end, we propose a compression strategy that targets  $\mathbf{b}$ . The update of  $\mathbf{b}^{(\ell+1)}$  for a certain coordinate  $i$  will be discarded if both of the following conditions are satisfied: (i) if  $b_i^{(\ell)} = 0$ , indicating that the determinant  $|D_i\rangle$  has not been selected before; (ii)  $\Delta b_i^{(\ell+1)} \leq \tau$ , with  $\Delta \mathbf{b}^{(\ell+1)} := H\mathcal{E}_{\mathcal{I}^{(\ell+1)}}\mathbf{a}^{(\ell+1)}$ , meaning that the update is relatively small. For any determinant  $|D_i\rangle$  deemed unimportant, as long as both  $b_i$  and  $c_i$  remain zero, it will not be selected during the coordinate selection step. Thus, the size of variational space is controlled, and the wavefunction vector will converge into a subspace of the full CI space, consisting only of limited number of important determinants.

Notably, despite compressing the vector  $\mathbf{b}$ ,  $b_i$  remains accurate for every determinant  $|D_i\rangle$  with nonzero coefficients in  $\mathbf{c}$ , meaning it was selected at least once during the coordinate selection step. This is achieved by recalculating  $b_i^{(\ell+1)}$  for each selected determinant  $|D_i\rangle$  selected at the  $\ell$ -th iteration, using the following formula:

$$b_i^{(\ell+1)} = H_{i,:}\mathbf{c}^{(\ell+1)} = \sum_{j \in \mathcal{I}_H(i)} H_{i,j}c_j^{(\ell+1)}. \quad (23)$$

Once a determinant  $|D_i\rangle$  is selected and recalculated, updates to  $b_i$  will not be discarded again according to the compression rule. Therefore,  $\mathbf{b}$  is only compressed for determinants that have not yet been added to the variational space. This ensures that the Rayleigh quotient  $(\mathbf{c}^T H \mathbf{c}) / (\mathbf{c}^T \mathbf{c})$ , is accurately maintained in each iteration by

$$\frac{(\mathbf{c}^{(\ell)})^T H \mathbf{c}^{(\ell)}}{(\mathbf{c}^{(\ell)})^T \mathbf{c}^{(\ell)}} = \frac{(\mathbf{c}^{(\ell)})^T \mathbf{b}^{(\ell)}}{(\mathbf{c}^{(\ell)})^T \mathbf{c}^{(\ell)}},$$

since the compressed terms  $b_i$  always have associated  $c_i = 0$  and therefore do not contribute to the sum.

Both the numerator and denominator are stored in memory, and updated in each iteration via the following straight-forward update

rules:

$$\begin{aligned} (\mathbf{c}^{(\ell+1)})^T \mathbf{c}^{(\ell+1)} &\leftarrow (\gamma^{(\ell)})^2 (\mathbf{c}^{(\ell)})^T \mathbf{c}^{(\ell)} \\ &+ 2\gamma^{(\ell)} (\mathbf{a}^{(\ell)})^T (\mathcal{E}_{\mathcal{I}^{(\ell)}} \mathbf{c}^{(\ell)}) \\ &+ (\mathbf{a}^{(\ell)})^T \mathbf{a}^{(\ell)}, \end{aligned} \quad (24)$$

and

$$\begin{aligned} (\mathbf{c}^{(\ell+1)})^T \mathbf{b}^{(\ell+1)} &\leftarrow (\gamma^{(\ell)})^2 (\mathbf{c}^{(\ell)})^T \mathbf{b}^{(\ell)} \\ &+ 2\gamma^{(\ell)} (\mathbf{a}^{(\ell)})^T (\mathcal{E}_{\mathcal{I}^{(\ell)}} \mathbf{b}^{(\ell)}) \\ &+ (\mathbf{a}^{(\ell)})^T H \mathbf{a}^{(\ell)}. \end{aligned} \quad (25)$$

## 2.2.4 Proposed Multi-Coordinate Descent FCI Method

The following outlines the complete procedure for the Multi-Coordinate Descent FCI method.

1. Initialize  $\mathcal{I}^{(0)}$ , the set of determinants pre-selected before computation begins. In our case, we choose  $\mathcal{I}^{(0)} = \{|D_{\text{HF}}\rangle\}$ , which introduces only one non-zero entry in  $\mathbf{c}^{(1)}$ , simplifying the computation of  $\mathbf{b}^{(1)}$ . Set  $\ell = 1$ , initialize  $\mathbf{c}^{(1)}$ , and compute  $\mathbf{b}^{(1)} = H\mathbf{c}^{(1)}$ . Other initial vectors may be chosen, provided that  $(\mathbf{c}^{(1)})^T H \mathbf{c}^{(1)} < 0$  holds.
2. Select the index set  $\mathcal{I}^{(\ell)} = \{i_1^{(\ell)}, \dots, i_k^{(\ell)}\}$  according to (10).
3. Evaluate the matrix  $(Q^{(\ell)})^T H Q^{(\ell)}$  following (18). Compute its lowest eigenvalue and corresponding eigenvector  $\mathbf{z}^{(\ell)}$ , and then obtain the scaling factor  $\gamma^{(\ell)}$  using (19) and the stepsize vector  $\mathbf{a}^{(\ell)}$  via (20).
4. Update  $\mathbf{c}^{(\ell+1)}$ ,  $\mathbf{b}^{(\ell+1)}$ ,  $(\mathbf{c}^{(\ell+1)})^T \mathbf{c}^{(\ell+1)}$  and  $(\mathbf{c}^{(\ell+1)})^T \mathbf{b}^{(\ell+1)}$  according to (21), (22), (24) and (25). Use the compression technique based on a predefined threshold  $\tau$ . Recalculate  $b_i^{(\ell+1)}$  for  $i \in \mathcal{I}^{(\ell)}$  as in (23).
5. Repeat steps 2–4 with  $\ell \leftarrow \ell + 1$  until either a stopping criterion or the maximum iteration number is reached. In our implementation, we adopt the stopping criterion proposed in OptOrbFCI.<sup>22</sup> The moving average  $S$  of the stepsize norm is

tracked using a decay factor of  $\alpha = 0.99$ ,

$$S^{\ell+1} \leftarrow \alpha S^\ell + (1 - \alpha) \|\mathbf{a}^{(\ell+1)}\|.$$

The algorithm halts when  $S^{\ell+1}$  falls below a specified tolerance level. Other stopping criteria, such as monitoring the change of the Rayleigh quotient or the ratio of the number of nonzero coefficients in  $\mathbf{b}$  and  $\mathbf{c}$ ,<sup>17</sup> may also be applied.

### 3 Computational Implementation and Complexity Analysis

We will now provide implementation details of the algorithm, focusing on computationally expensive components and numerical stability issues, while conducting complexity analysis in the same time. In the following analysis, we denote  $N_H = \max_i \mathcal{I}_H(i)$  as the maximum number of nonzero entries in columns of the Hamiltonian matrix, which scales as  $\mathcal{O}(n_{\text{elec}}^2 n_{\text{orb}}^2)$ . We claim that the per-iteration complexity of our algorithm is  $\mathcal{O}(kN_H + k^3)$ , and  $\mathcal{O}(N_H + k^3)$  for each thread with shared memory parallelism.

The sparse vectors  $\mathbf{c}$  and  $\mathbf{b}$  are stored in a hashtable that allows parallel read/write operations<sup>23</sup> as in previous work.<sup>17</sup> For each entry of the hash table, its key is the Slater determinant  $|D_i\rangle$  encoded by an  $n_{\text{orb}}$ -bit binary string, and its value is a pair of double floating-point numbers  $c_i$  and  $b_i$ . Three additional scalars are also stored in memory and updated in each iteration: the inner products  $\mathbf{c}^T \mathbf{c}$ ,  $\mathbf{c}^T \mathbf{b}$  and the scaling factor  $\gamma$ . All the three quantities are stored in quadruple-precision floating point format to mitigate accumulated numerical errors, ensuring accuracy unless the number of iterations exceeds  $10^{16}$ .<sup>17</sup>

Note that the Hamiltonian matrix is never stored in memory: indeed, we evaluate each Hamiltonian entry on-the-fly. Different from other selected CI methods, this significantly reduces the storage cost of our algorithm, and allows us to utilize all available storage capacity to store the ground-state coefficient vector  $\mathbf{c}$

and its associated  $\mathbf{b} = H\mathbf{c}$  related to the residual.

Our implementation utilizes shared memory parallelism based on OpenMP. Specifically, we enable  $k$  threads where  $k$  is the number of coordinates we choose to update in each iteration.

In the coordinate pick stage (described in section 2.2.1), each thread handling determinant  $|D_i\rangle$  examines determinants in  $\mathcal{I}_H(i)$  to select  $k$  determinants with the largest value of  $[\nabla f(\mathbf{c})]_i$ . This step has a complexity of  $\mathcal{O}(N_H)$  for each thread, and  $\mathcal{O}(kN_H)$  in total. After this, the main thread selects the  $k$  largest determinants from  $k^2$  gathered from all the threads.

In the subproblem solve stage (described in section 2.2.2), we begin by constructing the  $(k+1)$ -dimensional matrix  $(Q^{(\ell)})^T H Q^{(\ell)}$  in (18). It is evident that computing  $(\tilde{\mathbf{y}}^{(\ell)})^T H \tilde{\mathbf{y}}^{(\ell)}$  and  $\mathcal{E}_{\mathcal{I}^{(\ell)}}^T H \tilde{\mathbf{y}}^{(\ell)}$  involves only  $\mathcal{O}(k^2)$  cost, whereas for  $\mathcal{E}_{\mathcal{I}^{(\ell)}}^T H \mathcal{E}_{\mathcal{I}^{(\ell)}}$ , we need to evaluate  $k^2$  Hamiltonian entries, each with complexity  $\mathcal{O}(n_{\text{orb}})$ . For the subsequent eigenvalue problem, we want to retrieve the smallest eigenvalue and its corresponding eigenvector of a  $(k+1)$ -dimensional symmetric matrix. A robust eigensolver like MRRR<sup>21</sup> yields such eigenpair at a cost of  $\mathcal{O}(k^3 + Tk^2)$  where  $T$  is the number of iteration steps, which is usually comparable to  $k$ .

Unfortunately, MRRR only guarantees that the extreme eigenvalue is converged to double precision, without guaranteeing the accuracy of each entry in the eigenvector. This could be problematic because the magnitudes of coordinates in the eigenvector can vary widely, and the small values of the stepsize vector might only have an accuracy of  $10^{-8}$ . To address this issue, we employ one step of inverse iteration conducted in quadruple precision to improve the accuracy of eigenvector, which again has a complexity of  $\mathcal{O}(k^3)$ .

Finally, during the variable update stage (described in section 2.2.3), each thread is assigned to calculate a local update of  $\mathbf{b}$  in the form  $\Delta \mathbf{b}^i = H_{:,i} a_i$ . Compression occurs at the thread level, skipping updates of coordinate  $j$  if  $b_j = 0$  and  $\Delta \mathbf{b}_j^i \leq \tau$ . In this process, each thread constructs the  $i$ -th column of  $H$ ,  $H_{:,i}$ , which is subsequently used to recalculate  $b_i^{(\ell+1)}$  as described in (23). The complexity of the vari-



Table 1: Computational cost for each step per thread and in total.  $N_H$  is defined as the maximum number of nonzero entries in any column of the Hamiltonian matrix, i.e.,  $N_H = \max_i \mathcal{I}_H(i)$ .

Step	Complexity per thread	Complexity in total
Coordinate pick	$\mathcal{O}(N_H + k^2)$	$\mathcal{O}(kN_H + k^2)$
Subproblem solve	$\mathcal{O}(k^3)$	$\mathcal{O}(k^3)$
Variable update	$\mathcal{O}(N_H)$	$\mathcal{O}(kN_H)$

able update step remains  $\mathcal{O}(N_H)$  per thread, resulting in a total complexity of  $\mathcal{O}(kN_H)$ . The prefactor is dominated by the computation cost of a single Hamiltonian entry, which scales with  $\mathcal{O}(n_{\text{orb}})$ .

Table 1 gives a summary of computational cost for each step per thread and in total.

## 4 Numerical Experiments

In this section, we conduct a series of numerical experiments to demonstrate the efficiency of the proposed algorithm – multi-coordinate descent FCI method (mCDFCI). First, we compute the ground-state energy of  $\text{N}_2$  using three different basis sets: cc-pVDZ, cc-pVTZ, and cc-pVQZ. As the number of orbitals increases, the calculated energies become more accurate, but the computational cost also rises. We test the computations using different numbers of cores and demonstrate the strong parallel scaling for big systems. Subsequently, we compare the convergence curve and computation time with the original CDFCI method, as well as other methods, namely SHCI, DMRG and i-FCIQMC (initiator-FCIQMC). After that, we turn our eyes on a bigger system, the chromium dimer  $\text{Cr}_2$  under the Ahlrichs SV basis at  $r = 1.5\text{\AA}$ , with 48 electrons and 84 spin-orbitals. This is a well-known multi-reference system because of the spin coupling of the 12 valence electrons. Finally, we benchmark the binding curve of nitrogen dimer under the cc-pVQZ basis, which consists of 220 spin-orbitals.

In all experiments, the orbitals and integrals are calculated via restricted Hartree-Fock (RHF) in PSI4 package<sup>24</sup> version 1.8. All energies are reported in the unit of Hartree (Ha).

The program is compiled using the GNU g++

compiler version 11.4.0 with the `-O3` optimization flag and its native OpenMP support. It is linked against LAPACK version 3.11.0 and OpenBLAS version 0.3.26 for numerical linear algebra computations.

### 4.1 Scalability and Performance Testing

The  $\text{N}_2$  molecule is considered a correlated system due to the significant role of electron correlation effects in accurately describing its electronic structure. We compute its ground-state energy using three different basis sets: cc-pVDZ (14e, 28o), cc-pVTZ (14e, 60o), and cc-pVQZ (14e, 110o). A detailed description of the system and the configurations used when running the CDFCI program is provided in Table 2. The experiments in this section were conducted on a system equipped with two AMD EPYC 9754 128-core processors and 1.5 TB of memory.

In the multi-threaded implementation of CDFCI (mCDFCI), we define *effective iterations* as the product of the number of iterations and the number of determinants updated, ensuring that mCDFCI performs an equivalent workload regardless of the number of threads. Notably, in our experiments, while different values of  $k$  produce distinct energy descent trajectories, the energy values after the same number of effective iterations remain consistent, irrespective of the number of threads used. Specifically, for the cc-pVDZ basis, the maximum difference between energy values was  $4.84 \times 10^{-7}$  Ha, while for cc-pVTZ and cc-pVQZ, the differences were  $2.66 \times 10^{-6}$  Ha and  $9.09 \times 10^{-6}$  Ha, respectively. All of these differences are smaller than  $10^{-5}$  Ha, confirming the robustness and stability of the method.

Figure 2 shows the runtime of mCDFCI over

Table 2: Description of the basis sets, configurations, thresholds, and average nonzero per column used for  $N_2$  in section 4.1.  $N_H$  is defined as the maximum number of nonzero entries in any column of the Hamiltonian matrix, i.e.,  $N_H = \max_i \mathcal{I}_H(i)$ .

Basis Set	Electrons	Spin Orbitals	Threshold $\tau$	$N_H$
cc-pVDZ	14	56	$5 \times 10^{-7}$	$< 4 \times 10^3$
cc-pVTZ	14	120	$5 \times 10^{-6}$	$< 3 \times 10^4$
cc-pVQZ	14	220	$5 \times 10^{-5}$	$< 8 \times 10^4$

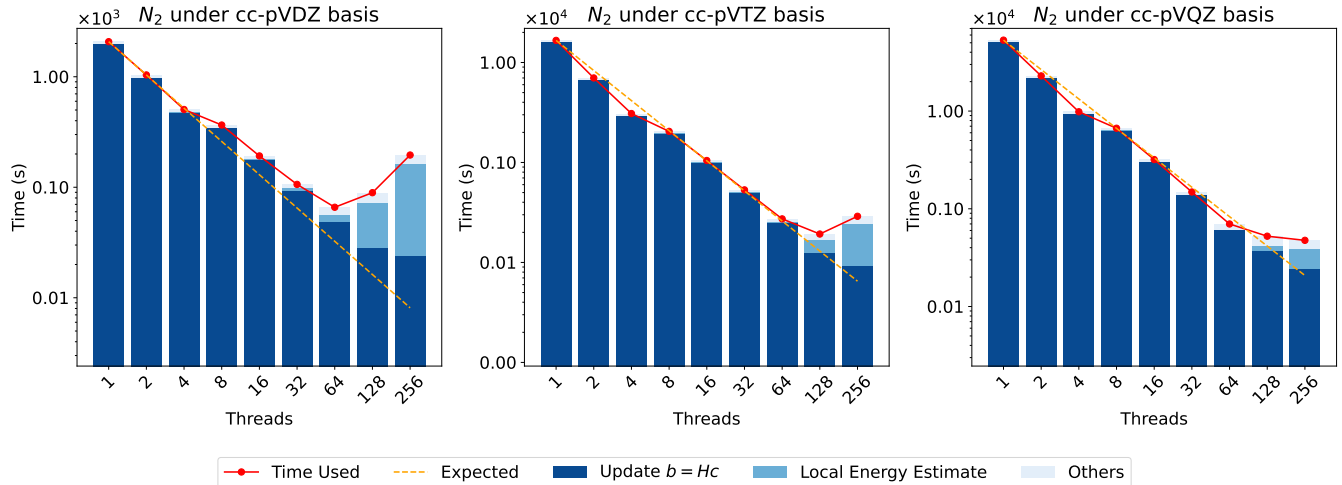


Figure 2: Comparison of runtime for the  $N_2$  molecule with different basis sets (cc-pVDZ, cc-pVTZ, and cc-pVQZ) using various numbers of threads. Each subplot represents a different basis set. The bar charts show the time in seconds spent on specific computational steps, including updating  $\mathbf{b} = H\mathbf{c}$ , local energy estimation, and other operations. The red dots on the line plot show the total time usage, while the yellow dashed line represents the ideal scaling behavior (expected performance improvement with increased threads).

1024K effective iterations, evaluated across a range of thread counts from 1 to 256. Detailed data supporting these results can be found in Appendix B. In every case, the dominant computational cost stems from the update of the vector  $\mathbf{b} = H\mathbf{c}$ , while the time for the local energy estimation, which is not parallelized, increases as the thread count rises. This increase is particularly noticeable for smaller systems, such as cc-pVDZ, where the computational time grows significantly beyond 64 threads.

For larger systems, strong parallel scalability is observed up to 128 threads, with instances of superlinear speedup. This performance gain is attributed to the hashtable we use, which is specifically designed and optimized for multi-threaded workloads. When focusing solely on the time taken to update the hash table and

disregarding the local energy estimation, it is clear that the update of the  $\mathbf{b}$  vector is highly parallelizable.

## 4.2 Numerical Results with $C_2$ and $N_2$

In this section, we compare the performance of our method with other FCI methods: SHCI, DMRG and i-FCIQMC, all with parallel support and using the same amount of computing resources. We test all the algorithms on two systems:  $C_2$  and  $N_2$  under the cc-pVDZ basis sets. The original CDFCI program<sup>25</sup> which supports OpenMP acceleration by parallelizing the update  $\mathbf{b} = H\mathbf{c}$ , is also tested here and renamed as sCDFCI (single-coordinate descent FCI) for comparison with

our new method mCDFCI (multi-coordinate descent FCI). SHCI, DMRG and i-FCIQMC calculations were performed using the Arrow code,<sup>26</sup> the Block2 code<sup>27</sup> and the NECI code,<sup>28</sup> respectively. All programs were compiled using the GNU g++ compiler (version 11.4.0) with the -O3 optimization flag. Native support for OpenMP was utilized, and MPI support was provided by MPICH (version 4.2.0). All programs were restricted to use 64 cores. CDFCI, SHCI, and DMRG were executed with 64 threads each, while i-FCIQMC, which supports only MPI parallelization, was executed with 64 MPI processes. Apart from the parallelization configurations enabled in our study, we used the same experimental settings as described in Wang et al.<sup>17</sup>. Specifically, SHCI was run with different thresholds  $\varepsilon_1$ , DMRG with varying maximum bond dimensions  $M$ , and i-FCIQMC with different numbers of walkers  $m$ . For i-FCIQMC, in addition to the default parameters, the initiator threshold was set to 3.0 and the number of iterations was set to 30,000 to ensure convergence by observation of clear plateaus in the diagnostic plots. The Hartree-Fock state was used as the initial wavefunction for all algorithms except DMRG, which has its own warm-up algorithm. In all cases, the energy is reported without any perturbation or extrapolation postcalculations. Variational energy is reported for CDFCI, SHCI and DMRG, while average projected energy is reported for i-FCIQMC.

Table 3 and Table 4 demonstrates the convergence behavior of the  $C_2$  and  $N_2$  molecule respectively, executed by different methods. Each method was evaluated with specific parameter values, and the results are documented in terms of absolute error, memory consumption in gigabytes (GB), execution time in seconds, and a comparison with the mCDFCI algorithm regarding execution time and relative ratio. From a broader perspective, there are significant differences in time and memory usage among the various algorithms, which we will examine in detail.

The proposed algorithm, mCDFCI, achieves chemical accuracy for the  $C_2$  molecule in less than one minute while using only 6 GB of mem-

ory. Subsequently, the energy continues to decrease at a linear rate. The expansion of the primary variational space slows down once the absolute error is less than  $10^{-5}$ . The wavefunction converges to a subspace of the full CI space according to the current truncation threshold  $\tau = 3 \times 10^{-8}$ . For the  $N_2$  molecule, mCDFCI exhibits similar behavior for threshold  $\tau = 5 \times 10^{-7}$ .

Compared to sCDFCI, which updates only one determinant per iteration, mCDFCI descends much faster and utilizes a smaller subspace at the start of the iterations. This demonstrates the efficiency of mCDFCI in capturing important determinants. Towards the end of the iterations, the effective iterations of mCDFCI and sCDFCI are comparable. However, mCDFCI still shows approximately three times the acceleration, highlighting the enhanced parallelization power utilized by our approach.

SHCI also adopts the concept of selected CI but employs a different data structure compared to ours. After selecting determinants based on an importance measure from the Hamiltonian matrix elements connected to the reference determinant, SHCI extracts a submatrix and directly diagonalizes it to find the smallest eigenpair. The efficiency of the SHCI algorithm can be attributed to the powerful Davidson algorithm, the one-time evaluation of the Hamiltonian matrix, and the contiguous memory read/write operations. Additionally, multi-threading is particularly effective for computing matrix-vector multiplications, making the method highly parallel and further boosting the performance. These factors enable SHCI to exhibit speedups over mCDFCI, especially when the required accuracy is low. However, the storage of the Hamiltonian submatrix leads to high storage costs, particularly when high accuracy is required. On the other hand, when  $\varepsilon_1 = 1 \times 10^5$ , SHCI uses 3,324,630 determinants to reach an accuracy of  $1.1 \times 10^{-4}$  Ha, whereas mCDFCI uses only 2,022,447 determinants to achieve the same accuracy. In this case, mCDFCI uses approximately 40% fewer determinants than SHCI to attain the same level of precision.

DMRG, which models the wavefunction using

Table 3: Convergence of ground-state energy for  $C_2$ . The reference ground-state energy is  $-75.7319615$  Ha. The absolute error is the difference between the reported energy and the reference ground-state energy. For i-FCIQMC, this error is based on the average projected energy, with uncertainty reported as given.

Algorithm	Parameter	Absolute Error	Mem(GB)	Time(s)	mCDFCI	
					Time(s)	Ratio
mCDFCI	$\tau = 3.0 \times 10^{-8}$	$1.0 \times 10^{-2}$	1.5	3.8	-	
		$1.0 \times 10^{-3}$	6.0	17.2	-	
		$1.0 \times 10^{-4}$	24.0	123.4	-	
		$1.0 \times 10^{-5}$	48.0	603.7	-	
		$1.0 \times 10^{-6}$	48.0	2332.3	-	
sCDFCI	$\varepsilon = 3.0 \times 10^{-8}$	$1.0 \times 10^{-2}$	3.0	14.7	3.8	$3.87\times$
		$1.0 \times 10^{-3}$	6.0	55.0	17.2	$3.20\times$
		$1.0 \times 10^{-4}$	24.0	374.3	123.4	$3.03\times$
		$1.0 \times 10^{-5}$	48.0	1779.7	603.7	$2.95\times$
		$1.0 \times 10^{-6}$	48.0	6906.0	2332.3	$2.96\times$
SHCI	$\varepsilon_1 = 1.0 \times 10^{-4}$	$1.5 \times 10^{-3}$	16.1	3.3	14.0	$0.23\times$
	$\varepsilon_1 = 5.0 \times 10^{-5}$	$7.6 \times 10^{-4}$	17.5	7.3	23.7	$0.31\times$
	$\varepsilon_1 = 1.0 \times 10^{-5}$	$1.1 \times 10^{-4}$	32.6	53.9	113.2	$0.48\times$
	$\varepsilon_1 = 5.0 \times 10^{-6}$	$4.6 \times 10^{-5}$	54.2	126.0	219.4	$0.57\times$
	$\varepsilon_1 = 1.0 \times 10^{-6}$	$4.7 \times 10^{-6}$	238.1	845.0	954.1	$0.89\times$
DMRG	$\max M = 500$	$6.9 \times 10^{-4}$	0.2	106.9	23.7	$4.52\times$
	$\max M = 1000$	$1.5 \times 10^{-4}$	0.8	345.2	92.7	$3.72\times$
	$\max M = 2000$	$1.9 \times 10^{-5}$	3.1	1130.1	394.9	$2.86\times$
	$\max M = 4000$	$2.1 \times 10^{-6}$	11.5	3848.3	1549.2	$2.48\times$
i-FCIQMC	$m = 10000$	$5.1 \pm 2.4 \times 10^{-3}$	0.049	7.0	3.8	$1.84\times$
	$m = 50000$	$1.6 \pm 1.3 \times 10^{-3}$	0.049	18.1	10.6	$1.71\times$
	$m = 100000$	$3.3 \pm 0.9 \times 10^{-3}$	0.049	31.1	7.2	$4.33\times$
	$m = 500000$	$1.7 \pm 7.0 \times 10^{-4}$	0.050	113.0	82.1	$1.38\times$
	$m = 1000000$	$9.6 \pm 3.3 \times 10^{-4}$	0.051	203.5	17.2	$11.83\times$

a matrix product state form, has a lower memory footprint than mCDFCI due to its storage cost of  $\mathcal{O}(n_{\text{orb}}M^2)$ , where  $n_{\text{orb}}$  is the number of orbitals and  $M$  the maximum bond dimension. However, mCDFCI achieves faster convergence compared to DMRG, particularly when targeting moderate accuracy. The difference in convergence speed decreases as higher accuracy is required, but mCDFCI remains more efficient overall.

Finally, i-FCIQMC, a stochastic method that approximates the wavefunction using random walkers, requires significantly less memory than mCDFCI. While i-FCIQMC has minimal mem-

ory usage, typically only a few megabytes, its error decreases slowly as the number of walkers increases. While i-FCIQMC can converge faster for lower accuracy requirements, mCDFCI provides a more reliable and efficient solution when higher precision is needed.

### 4.3 All-Electron Chromium Dimer Calculation

We now turn our attention to the larger system of the chromium dimer, which consists of 48 electrons and 84 spin-orbitals. Transition metals play a pivotal role in catalysis, biochemistry,

Table 4: Convergence of ground-state energy for  $N_2$ . The reference ground-state energy is  $-109.2821721$  Ha. The absolute error is the difference between the reported energy and the reference ground-state energy. For i-FCIQMC, this error is based on the average projected energy, with uncertainty reported as given.

Algorithm	Parameter	Absolute Error	Mem(GB)	Time(s)	mCDFCI	
					Time(s)	Ratio
mCDFCI	$\tau = 5.0 \times 10^{-7}$	$1.0 \times 10^{-2}$	3.0	4.2	-	-
		$1.0 \times 10^{-3}$	12.0	31.8	-	-
		$1.0 \times 10^{-4}$	24.0	311.8	-	-
		$1.0 \times 10^{-5}$	24.0	1830.3	-	-
		$1.0 \times 10^{-6}$	24.0	5629.8	-	-
sCDFCI	$\varepsilon = 5.0 \times 10^{-7}$	$1.0 \times 10^{-2}$	6.0	19.2	4.2	4.57×
		$1.0 \times 10^{-3}$	12.0	87.5	31.8	2.75×
		$1.0 \times 10^{-4}$	24.0	829.7	311.8	2.66×
		$1.0 \times 10^{-5}$	24.0	4687.7	1830.3	2.56×
		$1.0 \times 10^{-6}$	24.0	14048.5	5629.8	2.50×
SHCI	$\varepsilon_1 = 1.0 \times 10^{-4}$	$1.6 \times 10^{-3}$	16.8	4.0	19.7	0.20×
	$\varepsilon_1 = 5.0 \times 10^{-5}$	$8.8 \times 10^{-4}$	18.9	10.9	40.0	0.27×
	$\varepsilon_1 = 1.0 \times 10^{-5}$	$1.9 \times 10^{-4}$	37.9	76.2	175.2	0.44×
	$\varepsilon_1 = 5.0 \times 10^{-6}$	$8.6 \times 10^{-5}$	68.2	183.4	353.3	0.52×
	$\varepsilon_1 = 1.0 \times 10^{-6}$	$1.0 \times 10^{-5}$	402.7	1753.8	1796.5	0.98×
DMRG	max $M = 500$	$1.2 \times 10^{-3}$	0.2	126.5	27.9	4.54×
	max $M = 1000$	$3.1 \times 10^{-4}$	0.8	427.3	114.2	3.74×
	max $M = 2000$	$6.2 \times 10^{-5}$	3.1	1405.8	470.7	2.99×
	max $M = 4000$	$8.9 \times 10^{-6}$	11.8	4940.7	1976.8	2.50×
i-FCIQMC	$m = 10000$	$6.0 \pm 2.1 \times 10^{-3}$	0.135	21.2	4.2	5.04×
	$m = 50000$	$1.4 \pm 0.9 \times 10^{-3}$	0.135	65.1	23.9	2.72×
	$m = 100000$	$3.9 \pm 5.2 \times 10^{-4}$	0.135	114.1	91.2	1.25×
	$m = 500000$	$4.8 \pm 2.7 \times 10^{-4}$	0.136	474.6	71.8	6.61×
	$m = 1000000$	$2.9 \pm 2.2 \times 10^{-4}$	0.137	896.2	118.1	7.59×

and the energy sciences, but the complex electronic structure of d-shells presents significant challenges for modeling and understanding such processes.<sup>29</sup>

In the case of the chromium dimer, the high electron correlation arises from two main aspects: static correlation, which is due to the spin coupling of the 12 valence electrons, and dynamic correlation, which involves excitations of non-valence orbitals, such as the 3p electrons. To address this challenge, we computed the all-electron chromium dimer ground state at a bond length of 1.5 Å using the Ahlrichs SV basis set.

Figure 3 illustrates the energy decrease and time usage for running  $2 \times 10^7$  iterations using 128 threads. In this setup, 128 determinants are selected in each iteration, for either addition to the variational space or updating their associated values. The final number of determinants in the variational wavefunction is approximately  $2 \times 10^9$ .

The red curve in the plot represents the energy error (in Hartree) as a function of the number of iterations. This error decreases rapidly to the level of  $10^{-3}$  within several hours, before converging towards the ground-state energy at a steady linear rate.

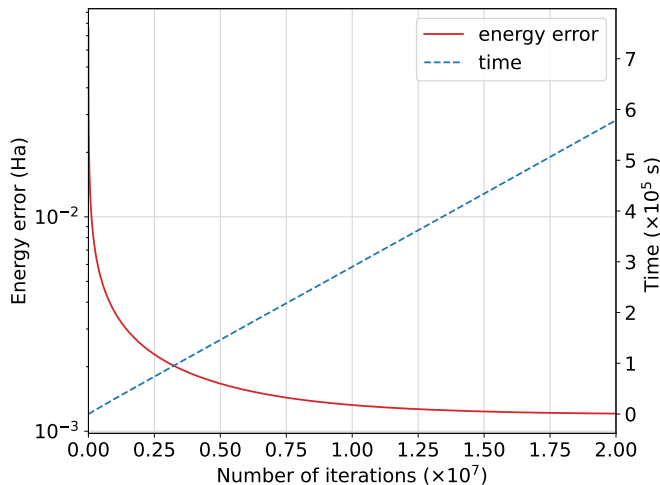


Figure 3: Convergence of ground-state energy for the  $\text{Cr}_2$  molecule under Ahlrichs SV basis. The threshold is set to  $3.7 \times 10^{-5}$  and the reference ground-state energy is  $-2086.444784$  Ha, obtained via extrapolated DMRG.<sup>30</sup> The energy error is computed as the absolute difference between the current variational energy (Rayleigh quotient) and the reference ground-state energy.

The blue dashed curve in the plot shows the total time elapsed as a function of the number of iterations, measured in seconds ( $\times 10^5$ ). A total of  $2 \times 10^7$  iterations takes around  $6 \times 10^5$  seconds, which is roughly one week. The linear trend indicates that the time per iteration remains relatively constant. This consistency is due to the number of nonzeros in each column of the Hamiltonian matrix being similar (around  $3 \times 10^4$ ), leading to a nearly constant computational cost per iteration (See Table 1 for complexity analysis). This predictable linear increase in time per iteration allows users to estimate the remaining computation time easily, demonstrating the practicality of the CD-FCI algorithm.

Compared to the previous CDFCI algorithm with single-coordinate updates, which achieved an energy of  $-2086.443565$  Ha after one month of computation,<sup>17</sup> we reached the same level of accuracy in just 5.8 days, despite using different computing environments. Additionally, we obtained a more accurate energy of  $-2086.443581$  Ha in approximately 8.8 days.

## 4.4 Binding Curve of $\text{N}_2$ under cc-pVQZ Basis

Finally, we benchmark the all-electron nitrogen binding curve under cc-pVQZ basis. The problem is challenging due to the complexity of accurately capturing the strong electron correlation in the triple bond of  $\text{N}_2$ . The large cc-pVQZ basis set increases computational cost, and all-electron calculations add further complexity by requiring the explicit treatment of core electrons. We adopt  $\tau = 5 \times 10^{-6}$  for mCDFCI truncation, use 128 threads, and run 1,000,000 iterations. The bond length is varied from  $1.5$  to  $4.5 a_0$ . Each configuration on the binding curve takes roughly 18 hours to achieve chemical accuracy.

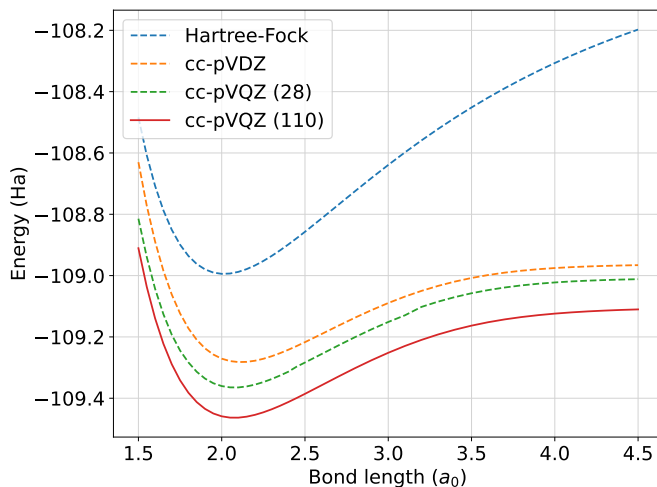


Figure 4: ground-state energy versus bond length for  $\text{N}_2$  using different basis sets. cc-pVQZ (110) refers to the full, uncompressed cc-pVQZ basis set, while cc-pVQZ (28) refers to the compressed set of orbitals generated by OptOrbFCI. The mCDFCI truncation threshold  $\tau = 5 \times 10^{-6}$  and stopping criteria of  $1 \times 10^{-5}$  are applied.

Figure 4 displays a smooth, standard-shaped binding curve (shown in red) for  $\text{N}_2$  calculated using the mCDFCI method with a full cc-pVQZ basis set (110 orbitals). The curve reaches its minimum at the equilibrium bond length of  $r = 2.118 a_0$ , which corresponds to the optimal bond length where the energy is minimized. This red curve is compared against other computational results, including the Hartree-Fock

approximation (blue dashed line) and CDFCI calculations using a reduced orbital set generated from cc-pVQZ, which is compressed to 28 selected orbitals (green dashed curve).

The Hartree–Fock method overestimates the total energy, particularly at longer bond lengths, due to its inability to capture dynamic electron correlation and its inherent inclusion of ionic character.<sup>31</sup> The green dashed curve represents results from the OptOrbFCI method,<sup>22</sup> which uses a rotation and compression of the full cc-pVQZ basis set into 28 selected orbitals. This method was employed to reduce the computational cost while retaining the essential characteristics of the electronic structure of the system. Despite the reduction in the number of orbitals, OptOrbFCI produces an energy profile closer to the full cc-pVQZ calculation than the cc-pVDZ approximation, showing that the selected orbitals capture most of the correlation effects. However, the slight increase in energy compared to the full cc-pVQZ curve reflects the inherent trade-off between computational efficiency and accuracy when compressing the basis set.

Appendix C lists all the variational energies corresponding to each bond length and configuration shown in the figure, providing a detailed comparison of the methods and basis sets. This comparison underscores the importance of increasing the basis set size to achieve basis set convergence in quantum chemical calculations.

## 5 Conclusion

This paper presents a novel algorithm, multi-coordinate Descent FCI method, for solving the full configuration interaction (FCI) problem in electronic structure calculations. The algorithm reformulates the FCI eigenvalue problem as an unconstrained optimization problem and employs a multi-coordinate descent approach to update the optimization variable. Additionally, the algorithm introduces a compression strategy to control the size of the variational space.

The method demonstrates efficiency and accuracy through various benchmarks, including the computation of an accurate benchmark en-

ergy for the chromium dimer and the binding curve of nitrogen dimer. The results show up to 79.3% parallel efficiency on 128 cores, as well as significant speedup compared to previous methods. Overall, the Multi-Coordinate Descent FCI method presents a promising approach for solving the FCI problem in electronic structure calculations, with improved efficiency, accuracy, and parallelization capability, making it suitable for larger systems and more accurate approximations.

Since the current algorithm focuses on improving the variational stage of selected CI, our immediate future work will involve adding a perturbation stage to the current algorithm. Another direction will be to combine the current results with orbital optimization, as it is well known that optimized orbitals lead to faster convergence.<sup>22,32,33</sup> Several approaches for computing excited states within the FCI framework have been developed.<sup>34–38</sup> These methods, often extensions of ground-state algorithms, have demonstrated success in accurately treating excited states. Recently, Wang et al. introduced xCDFCI,<sup>39</sup> an efficient extension of CDFCI designed specifically for low-lying excited states in molecules. We aim to adapt our techniques for excited-state computations as well.

Regarding parallel capacity, extending our current shared-memory implementation to a distributed-memory one with MPI enabled is an interesting prospect, as it would further increase computational capacity and leverage memory load. A well-implemented distributed memory setup is under investigation.

## Acknowledgments

The authors thank Jianfeng Lu and Zhe Wang for their helpful discussions and valuable insights during the course of this work. This research was supported by the National Natural Science Foundation of China (NSFC) under grant numbers 12271109 and 71991471, the National Key R&D Program of China under grant 2020YFA0711902, the Science and Technology Commission of Shanghai Municipi-

pality (STCSM) under grant numbers 22TQ017 and 24DP2600100, and the Shanghai Institute for Mathematics and Interdisciplinary Sciences (SIMIS) under grant number SIMIS-ID-2024-(CN). The authors are also grateful for the resources and facilities provided by NSFC, the National Key R&D Program of China, STCSM, and SIMIS, which were essential for the completion of this work.

## References

- (1) White, S. R.; Martin, R. L. Ab initio quantum chemistry using the density matrix renormalization group. *The Journal of Chemical Physics* **1999**, *110*, 4127–4130.
- (2) Chan, G. K.-L.; Head-Gordon, M. Highly correlated calculations with a polynomial cost algorithm: A study of the density matrix renormalization group. *The Journal of Chemical Physics* **2002**, *116*, 4462–4476.
- (3) Chan, G. K.-L.; Sharma, S. The Density Matrix Renormalization Group in Quantum Chemistry. *Annual Review of Physical Chemistry* **2011**, *62*, 465–481.
- (4) Schollwöck, U. The density-matrix renormalization group in the age of matrix product states. *Annals of Physics* **2011**, *326*, 96–192.
- (5) Keller, S.; Dolfi, M.; Troyer, M.; Reiher, M. An efficient matrix product operator representation of the quantum chemical Hamiltonian. *The Journal of Chemical Physics* **2015**, *143*, 244118.
- (6) Booth, G. H.; Thom, A. J. W.; Alavi, A. Fermion Monte Carlo without fixed nodes: A game of life, death, and annihilation in Slater determinant space. *The Journal of Chemical Physics* **2009**, *131*, 054106.
- (7) Ghanem, K.; Lozovoi, A. Y.; Alavi, A. Unbiasing the initiator approximation in full configuration interaction quantum Monte Carlo. *The Journal of Chemical Physics* **2019**, *151*, 224108.
- (8) Blunt, N. S.; Thom, A. J. W.; Scott, C. J. C. Preconditioning and Perturbative Estimators in Full Configuration Interaction Quantum Monte Carlo. *Journal of Chemical Theory and Computation* **2019**, *15*, 3537–3551.
- (9) Cleland, D.; Booth, G. H.; Alavi, A. Communications: Survival of the fittest: Accelerating convergence in full configuration-interaction quantum Monte Carlo. *The Journal of Chemical Physics* **2010**, *132*, 041103.
- (10) Yang, M.; Pahl, E.; Brand, J. Improved walker population control for full configuration interaction quantum Monte Carlo. *The Journal of Chemical Physics* **2020**, *153*, 174103.
- (11) Eriksen, J. J. The Shape of Full Configuration Interaction to Come. *The Journal of Physical Chemistry Letters* **2021**, *12*, 418–432.
- (12) Huron, B.; Malrieu, J.; Rancurel, P. Iterative perturbation calculations of ground and excited state energies from multiconfigurational zeroth-order wavefunctions. *The Journal of Chemical Physics* **1973**, *58*, 5745–5759.
- (13) Tubman, N. M.; Lee, J.; Takeshita, T. Y.; Head-Gordon, M.; Whaley, K. B. A deterministic alternative to the full configuration interaction quantum Monte Carlo method. *The Journal of Chemical Physics* **2016**, *145*.
- (14) Holmes, A. A.; Tubman, N. M.; Umrigar, C. Heat-bath configuration interaction: An efficient selected configuration interaction algorithm inspired by heat-bath sampling. *Journal of Chemical Theory and Computation* **2016**, *12*, 3674–3680.
- (15) Sharma, S.; Holmes, A. A.; Jeanmairat, G.; Alavi, A.; Umrigar, C. J. Semistochastic heat-bath configuration interaction method: Selected configuration



- interaction with semistochastic perturbation theory. *Journal of Chemical Theory and Computation* **2017**, *13*, 1595–1604.
- (16) Li, J.; Otten, M.; Holmes, A. A.; Sharma, S.; Umrigar, C. J. Fast Semistochastic Heat-Bath Configuration Interaction. *The Journal of Chemical Physics* **2018**, *148*, 214110.
- (17) Wang, Z.; Li, Y.; Lu, J. Coordinate Descent Full Configuration Interaction. *Journal of Chemical Theory and Computation* **2019**, *15*, 3558–3569.
- (18) Greene, S. M.; Webber, R. J.; Weare, J.; Berkelbach, T. C. Improved Fast Randomized Iteration Approach to Full Configuration Interaction. *Journal of Chemical Theory and Computation* **2020**, *16*, 5572–5585.
- (19) Goings, J. J.; Hu, H.; Yang, C.; Li, X. Reinforcement Learning Configuration Interaction. *Journal of Chemical Theory and Computation* **2021**, *17*, 5482–5491.
- (20) Li, Y.; Lu, J.; Wang, Z. Coordinate-Wise Descent Methods for Leading Eigenvalue Problem. *SIAM Journal on Scientific Computing* **2019**, *41*, A2681–A2716.
- (21) Dhillon, I. S.; Parlett, B. N.; Vömel, C. The design and implementation of the MRRR algorithm. *ACM Transactions on Mathematical Software* **2006**, *32*, 533–560.
- (22) Li, Y.; Lu, J. Optimal Orbital Selection for Full Configuration Interaction (OptOrbFCI): Pursuing the Basis Set Limit under a Budget. *Journal of Chemical Theory and Computation* **2020**, *16*, 6207–6221.
- (23) A high-performance, concurrent hash table. <https://github.com/efficient/libcuckoo>, Accessed: 2024-05-07.
- (24) Turney, J. M. et al. Psi4: an open-source ab initio electronic structure program. *WIREs Computational Molecular Science* **2012**, *2*, 556–565.
- (25) C++ implemented Coordinate Descent Full Configuration Interaction (CDFCI) package for quantum chemistry calculation. <https://github.com/quantum/CDFCI>, Accessed: 2024-06-21.
- (26) Arrow - Fast Semistochastic Heat Bath Configuration Interaction Solver (SHCI). <https://github.com/QMC-Cornell/shci>, Accessed: 2024-06-21.
- (27) Efficient parallel quantum chemistry DMRG in MPO formalism. <https://github.com/block-hczhai/block2-preview>, Accessed: 2024-06-21.
- (28) Standalone NECI codebase designed for FCIQMC and other stochastic quantum chemistry methods. <https://github.com/quantum/CDFCI>, Accessed: 2024-06-21.
- (29) Larsson, H. R.; Zhai, H.; Umrigar, C. J.; Chan, G. K.-L. The Chromium Dimer: Closing a Chapter of Quantum Chemistry. *Journal of the American Chemical Society* **2022**, *144*, 15932–15937.
- (30) Olivares-Amaya, R.; Hu, W.; Nakatani, N.; Sharma, S.; Yang, J.; Chan, G. K.-L. The ab-initio density matrix renormalization group in practice. *The Journal of Chemical Physics* **2015**, *142*, 034102.
- (31) Kreplin, D. A. Multiconfiguration Self-consistent Field Methods for Large Molecules. Ph.D. thesis, Universität Stuttgart, 2020.
- (32) Smith, J. E. T.; Mussard, B.; Holmes, A. A.; Sharma, S. Cheap and Near Exact CASSCF with Large Active Spaces. *Journal of Chemical Theory and Computation* **2017**, *13*, 5468–5478.
- (33) Li, J.; Yao, Y.; Holmes, A. A.; Otten, M.; Sun, Q.; Sharma, S.; Umrigar, C. J. Accurate many-body electronic structure near the basis set limit: Application to the chromium dimer. *Physical Review Research* **2020**, *2*, 012015.

- (34) Blunt, N. S.; Smart, S. D.; Booth, G. H.; Alavi, A. An excited-state approach within full configuration interaction quantum Monte Carlo. *The Journal of Chemical Physics* **2015**, *143*, 134117.
- (35) Holmes, A. A.; Umrigar, C. J.; Sharma, S. Excited states using semistochastic heat-bath configuration interaction. *The Journal of Chemical Physics* **2017**, *147*, 164111.
- (36) Schriber, J. B.; Evangelista, F. A. Adaptive configuration interaction for computing challenging electronic excited states with tunable accuracy. *Journal of Chemical Theory and Computation* **2017**, *13*, 5354–5366.
- (37) Gao, W.; Li, Y.; Lu, B. Triangularized orthogonalization-free method for solving extreme eigenvalue problems. *Journal of Scientific Computing* **2022**, *93*.
- (38) Gao, W.; Li, Y.; Shen, H. Weighted trace-penalty minimization for full configuration interaction. *SIAM Journal on Scientific Computing* **2024**, *46*, A179–A203.
- (39) Wang, Z.; Zhang, Z.; Lu, J.; Li, Y. Coordinate Descent Full Configuration Interaction for Excited States. *Journal of Chemical Theory and Computation* **2023**, *19*, 7731–7739.

## A Proof in Section 2.2.2

We prove  $\lambda_{\min}((Q^{(\ell+1)})^T H Q^{(\ell+1)}) < 0$  as long as we choose an initial vector  $\mathbf{c}^{(1)}$  such that  $(\mathbf{c}^{(1)})^T H \mathbf{c}^{(1)} < 0$ , where  $Q^{(\ell+1)}$  is defined in (13). The proof uses induction and contradiction. In simple terms, if we assume  $(Q^{(\ell+1)})^T H Q^{(\ell+1)}$  is positive semi-definite, then the minimization problem will attain its minimum when the optimization vector is zero. However, we can always find a vector that leads to a smaller value, thus contradicting our initial assumption.

We first show that if  $\mathbf{c}^{(1)}$  is chosen such that  $(\mathbf{c}^{(1)})^T H \mathbf{c}^{(1)} < 0$ , then, starting from the first iteration, we have  $\lambda_{\min}((Q^{(1)})^T H Q^{(1)}) < 0$ . Conversely, if all eigenvalues of  $(Q^{(1)})^T H Q^{(1)}$  are non-negative, solving the minimization problem (16) yields  $\mathbf{z}^{(1)} = \mathbf{0}$  and  $f(\mathbf{z}^{(1)}) = \|H\|_{\text{F}}^2$ . However,  $\|H\|_{\text{F}}^2$  is clearly not the minimal point for  $f(\mathbf{c}^{(2)})$ . To see this, we take

$$\gamma^{(1)} = \frac{\sqrt{-(\mathbf{c}^{(1)})^T H \mathbf{c}^{(1)}}}{(\mathbf{c}^{(1)})^T \mathbf{c}^{(1)}},$$

and  $\mathbf{a}^{(1)} = \mathbf{0}$ , we have

$$\begin{aligned} f(\mathbf{c}^{(2)}) &= \|H + \gamma^{(1)} \mathbf{c}^{(1)} (\gamma^{(1)} \mathbf{c}^{(1)})^T\|_{\text{F}}^2 \\ &= \|H\|_{\text{F}}^2 + 2(\gamma^{(1)})^2 (\mathbf{c}^{(1)})^T H \mathbf{c}^{(1)} \\ &\quad + (\gamma^{(1)})^4 ((\mathbf{c}^{(1)})^T \mathbf{c}^{(1)})^2 \\ &= \|H\|_{\text{F}}^2 - \left( \frac{(\mathbf{c}^{(1)})^T H \mathbf{c}^{(1)}}{(\mathbf{c}^{(1)})^T \mathbf{c}^{(1)}} \right)^2 \\ &< \|H\|_{\text{F}}^2. \end{aligned}$$

Thus  $(Q^{(1)})^T H Q^{(1)}$  must have at least one negative eigenvalue.

We then show that if, in the previous step, we have  $\lambda_{\min}((Q^{(\ell)})^T H Q^{(\ell)}) < 0$ , it follows that  $\lambda_{\min}((Q^{(\ell+1)})^T H Q^{(\ell+1)}) < 0$ . The reasoning is similar to above. Suppose this is not true, such that all eigenvalues of  $(Q^{(\ell+1)})^T H Q^{(\ell+1)}$  are non-negative. Solving the minimization problem (16) would result in  $\mathbf{z}^{(\ell+1)} = \mathbf{0}$  and  $f(\mathbf{z}^{(\ell+1)}) = \|H\|_{\text{F}}^2$ . However, this is impossible. To see why, consider taking  $\gamma^{(\ell+1)} = 1$  and  $\mathbf{a}^{(\ell+1)} = \mathbf{0}$ . In this case, the function  $f(\mathbf{c}^{(\ell+1)})$  would have the same value as in the previous

iteration:

$$\begin{aligned} f(\mathbf{c}^{(\ell+1)}) &= \|H + \mathbf{c}^{(\ell)}(\mathbf{c}^{(\ell)})^T\|_F^2 \\ &= \|H\|_F^2 - (\lambda_{\min}((Q^{(\ell)})^T H Q^{(\ell)}))^2 \\ &< \|H\|_F^2. \end{aligned}$$

This demonstrates that the objective function value must decrease in each iteration. Additionally, in each iteration, we must have  $\lambda_{\min}((Q^{(\ell+1)})^T H Q^{(\ell+1)}) < 0$ .

## B Ground-State Energy Computation of N<sub>2</sub> Using Different Basis Sets

Tables 5 to 7 present the time taken by mCD-FCI for each basis set (cc-pVDZ, cc-pVTZ, and cc-pVQZ) across varying numbers of threads, as well as the corresponding parallel efficiency. These results highlight the scalability and efficiency of the multi-threaded implementation for each basis set.

Table 5: Time and Parallel Efficiency for Ground-State Energy of N<sub>2</sub> Using cc-pVDZ (14e, 28o)

Threads	Time (s)	Parallel Efficiency
1	2076.40	1.000
2	1038.48	1.000
4	505.32	1.027
8	365.66	0.710
16	192.09	0.676
32	106.10	0.612
64	65.91	0.492
128	89.31	0.182
256	195.71	0.041

## C N<sub>2</sub> Binding Curve Data for Bond Length and Energy

Table 8 shows the binding curve data for four sets of calculations: Hartree–Fock (HF), CD-

Table 6: Time and Parallel Efficiency for Ground-State Energy of N<sub>2</sub> Using cc-pVTZ (14e, 60o)

Threads	Time (s)	Parallel Efficiency
1	16626.01	1.000
2	7003.45	1.187
4	3084.88	1.347
8	2045.62	1.016
16	1045.78	0.994
32	531.91	0.977
64	272.70	0.953
128	192.42	0.675
256	289.45	0.224

Table 7: Time and Parallel Efficiency for Ground-State Energy of N<sub>2</sub> Using cc-pVQZ (14e, 110o)

Threads	Time (s)	Parallel Efficiency
1	53182.43	1.000
2	22897.89	1.161
4	9834.53	1.352
8	6669.42	0.997
16	3190.37	1.042
32	1485.38	1.119
64	699.20	1.188
128	524.26	0.793
256	475.64	0.437

FCI with the cc-pVDZ basis, CDFCI with the full cc-pVQZ (110 orbitals), and CDFCI with a reduced set of 28 compressed orbitals derived from the cc-pVQZ basis using the OptOrbFCI method.<sup>22</sup> The energies for HF were generated using the PSI4 package<sup>24</sup> version 1.8. The energies for the cc-pVDZ and cc-pVQZ (28) basis sets are cited from previous studies.<sup>17,22</sup> The table includes the bond lengths in atomic units ( $a_0$ ) and the corresponding ground-state energies in Hartree (Ha).

Table 8: Binding curve data for bond length and energy, showing the results from Hartree–Fock (HF), cc-pVDZ, and CDFCI with both the full cc-pVQZ basis (110 orbitals) and the compressed cc-pVQZ basis (28 orbitals).

Bond Length ( $a_0$ )	Hartree–Fock	cc-pVDZ	cc-pVQZ (28)	cc-pVQZ (110)
1.50	-108.484166	-108.630048	-108.814403	-108.910666
1.55	-108.607446	-108.771997	-108.939182	-109.036535
1.60	-108.707310	-108.888846	-109.042905	-109.139272
1.65	-108.787292	-108.984314	-109.126015	-109.222403
1.70	-108.850397	-109.061575	-109.192655	-109.288927
1.75	-108.899180	-109.123348	-109.244370	-109.341398
1.80	-108.935822	-109.171964	-109.283011	-109.381998
1.85	-108.962179	-109.209426	-109.313701	-109.412578
1.90	-108.979837	-109.237458	-109.335975	-109.434729
1.95	-108.990152	-109.257541	-109.351156	-109.449809
2.00	-108.994283	-109.270953	-109.360360	-109.458975
2.05	-108.993221	-109.278790	-109.364582	-109.463219
2.10	-108.987816	-109.281994	-109.364756	-109.463348
2.15	-108.978797	-109.281374	-109.361496	-109.460105
2.20	-108.966786	-109.277621	-109.355553	-109.454133
2.25	-108.952320	-109.271328	-109.347340	-109.445965
2.30	-108.935857	-109.263001	-109.337391	-109.436048
2.35	-108.917789	-109.253072	-109.325979	-109.424753
2.40	-108.898453	-109.241908	-109.313533	-109.412410
2.45	-108.878135	-109.229823	-109.297016	-109.399302
2.50	-108.857081	-109.217083	-109.283533	-109.385670
2.60	-108.813564	-109.190508	-109.255799	-109.357597
2.70	-108.769211	-109.163600	-109.227940	-109.329427
2.80	-108.724949	-109.137358	-109.200871	-109.302021
2.90	-108.681424	-109.112473	-109.175147	-109.275997
3.00	-108.639072	-109.089405	-109.151280	-109.251749
3.10	-108.598176	-109.068450	-109.129515	-109.229566
3.20	-108.558912	-109.049779	-109.102007	-109.209619
3.30	-108.521376	-109.033462	-109.084817	-109.191894
3.40	-108.485608	-109.019484	-109.070067	-109.176446
3.50	-108.451609	-109.007747	-109.057557	-109.163193
3.60	-108.419352	-108.998083	-109.047199	-109.152036
3.70	-108.388793	-108.990269	-109.038765	-109.142780
3.80	-108.359873	-108.984050	-109.031901	-109.135188
3.90	-108.332527	-108.979162	-109.026548	-109.129007
4.00	-108.306685	-108.975357	-109.022348	-109.123980
4.10	-108.282276	-108.972410	-109.018986	-109.119960
4.20	-108.259228	-108.970132	-109.016448	-109.116684
4.30	-108.237469	-108.968366	-109.014495	-109.114082
4.40	-108.216928	-108.966991	-109.012920	-109.111935
4.50	-108.197538	-108.965910	-109.011722	-109.110256